PERGAMON

Computers and Structures 69 (1998) 473–486

Computers & Structures

An investigation of non-linear dynamics of multilayered plates accounting for C_z^0 requirements

E. Carrera *, H. Krause [1]

Institute for Statics and Dynamics, University of Stuttgart, Germany

Received 26 January 1996; received in revised form 23 April 1998

Abstract

Concerning accurate modelling of multilayered thick plates, this paper investigates both zig-zag and interlaminar continuity effects, i.e. C_z^0 requirements, in the non-linear (in von Kármán sense) dynamics fields. The used model, denoted elsewhere by the acronym RMZC (Reissner–Mindlin, Zig-zag, Continuity) furnishes, as a particular case, both the CLT (Classical Lamination Theory) and the FSDT (First-order Shear Deformation Theory). Efficient finite element plate formulations of Reissner–Mindlin type have been introduced to derive approximate governing equations, which are then solved by employing Newton–Raphson linearization and Newmark time-integration methods. Different geometries, loading conditions and layouts have been considered in the numerical part. As for the static case, it has been confirmed that the RMZC model improves the FSDT results in the analysis of large amplitude vibrations of thick plates. In the case of thin plates, both models have led to similar results. Several examples have shown that CLT, as well as linear approximation, can lead to a poor description of the non-linear dynamical behaviour of laminated plates. Furthermore, by considering a steady-state solution of damped harmonic forced excitation, it has been found that in the case of unsymmetrically laminated plates, the linear solution can over- or underestimate the non-linear results, depending both on the magnitude and type of the applied loading.

1. Introduction

The application of advanced high stiffness/strength-to-weight composite material systems has played a key role in the success of the aerospace and aircraft industries. In fact, nowadays a major portion of curved and flat panels of modern aeroplanes (e.g. fuselage, wing and stabilizer panels) as well as space vehicles are made of composite materials. However, the analysis of multilayered structures is a complex task compared with conventional one-layer metallic structures. That is mainly due to the following three reasons: (1) anisotropic panels may exhibit coupling among membrane, torsional and bending strains; (2) advanced composite materials are characterized by weak transverse shear rigidities; and (3) the discontinuity of the mechanical characteristics along the panel thickness requires appropriate two-dimensional (2D) modelling.

Owing to the geometry of laminated structural components, 2D approaches have been extensively used to describe their response under various loading conditions. When applied to thick panels with high orthotropic ratio, the *Classical Lamination Theory* (CLT) and *Shear deformation theories of Reissner–Mindlin-type* (FSDT) have revealed their limits to analyse global and local characteristics, respectively [1]. Such a deficiency is mainly due to the fact that these two classical approaches do not describe the zig-zag form of the displacement field and do not fulfill interlaminar equilibria at each interface along the thickness of the panel. These two aspects, as denoted in Ref. [2], can be

* Corresponding author. Research Engineer. Visiting under GKKS grant. Permanent address: DIAS, Politecnico di Torino, Corso Duca degli Abruzzi 24, Italy. Tel.: + + 39-11-546-6836; Fax: + + 39-11-564-6899; E-mail: carrera@polito.it.

[1] Ph.D Student of GKKS.

0045-7949/98/$ - see front matter
PII: S0045-7949(98)00112-6

summarized in the C_z^0 requirements, i.e. C^0 continuity of transverse stresses and displacements (and not of their derivatives, which are, in general, discontinuous) along the z-direction. Many higher-order Shear Deformation Theories (HSDT) have been proposed with the aim to include totally or partially these requirements in the analysis. Exhaustive overviews on the topics can be found in Refs [3, 4], and more recently in Refs [2, 5].

Very often these structures are subjected to severe environmental conditions which necessitate the study of their non-linear response, i.e. large deflection, post-buckling, and large amplitude vibrations including non-linear panel flutter [6–11]. The analysis of their vibrational characteristics in the non-linear domain is of particular interest, as it leads to a better understanding of the behaviour of laminated structures and thus enables the full exploitation of their advantages. Nevertheless, non-linear dynamics is a cumbersome matter [12] and the interest on tools and results concerning multilayered structures is still increasing. Both analytical and approximate solution methods have been applied in the recent past to these aims. A short review is discussed in the following text. Early results were presented by Ambartsumyan [13], Hassert and Novinsky [14], Wu and Winson [15], Whitney and Leissa [16] and Bert [7]. A more recent, comprehensive study of the large amplitude free vibration of plates, using approximate analytical and numerical methods, has been presented by Sathyamoorthy [18]. Sun and Chin [19] recognized the effects of bending-extension coupling in the non-linear plate theory. Flexural vibration of cross-ply laminated plates were analysed by Chandra and Raju [20], Singh et al. [21] and Ganapathi et al. [22]. All of these studies were based on the CLT approach. Large displacements and finite rotations finite element, static analyses have been recently provided by Di and Ramm [23, 24]. Large amplitude finite element solutions accounting for the FSDT and HSDT theory were presented by Reddy and Chao [25] and Kant and Kommineni [26], respectively. Both models used in these papers do not address the C_z^0.

Anisotropy, higher-order modelling, geometric non-linearities and dynamics greatly increase the difficulties of finding numerical solutions. On the other hand, the progress made by the computational mechanics in the last three decades helps very much to subjugate the mentioned difficulties. In particular, finite element formulation provides a convenient method of solution for such laminated composites having complex geometries, structural damping, arbitrary static and dynamic loadings, as well as support conditions and layouts [27–31]. Efficient formulated plate elements accounting for C_z^0 requirements (transverse normal stress was neglected) have been recently presented in Ref. [32]. A mixed 2D mechanical model proposed by Murakami [33] was employed. This was denoted by the acronym RMZC *Reissner–Mindlin, Zig-zag, Continuity*. It was seen as the extension of the Reissner–Mindlin model to multilayered plate analysis. It assumes two independent fields along the plate thickness for the displacements and transverse shear stresses, respectively; the displacement model describes the zig-zag form for the in-plane components, while the stress field fulfills interlaminar equilibria. Standard displacement formulation was enforced by employing variationally consistent constitutive equations between stress and displacement unknowns, as in Ref. [2]. Von Kármán-type geometrical non-linearities were included in Refs [34, 35] to analyse the stress field in the static large deflection and postbuckling fields.

With the aim to investigate C_z^0 and large deflections in the dynamics field, the present work extends the RMZC model to non-linear dynamics of multilayered plates. The governing non-linear system of algebraic equations is solved by employing Newton–Raphson linearization and the Newmark scheme for time integration. Thick and thin, symmetrically and unsymmetrically, angle-ply and cross-ply laminated plates are analysed when subjected to in-plane and out-of-plane dynamic loadings. Shear deformation, C_z^0 and non-linear effects are made evident by comparing the RMZC, FSDT and CLT, as well as linear and non-linear results in most of the conducted investigations.

2. Description of the RMZC model

2.1. Preliminary

The geometry, notation and coordinate system of the laminated plates of N_l layers are shown in Fig. 1. The integer k denotes the layer number, starting from the top of the plate. The letters x and y denote the plate middle surface coordinates. Ω is the x, y plate domain. The lamina are assumed to be homogeneous and orthotropic, and the material is supposed to work in a linear elastic field. For convenience, several reference coordinates are introduced along the plate thickness: z is the global coordinate along the plate thickness h, z_k, ($z_k = z - z_{0k}$, z_{0k} denotes the distance of the middle surface of the kth layer from the x–y plane) denotes the local coordinate along the kth, layer thickness h_k, $\zeta = 2z/h$ and $\zeta_k = 2z_k/h_k$ are the non-dimensional global plate coordinate and local kth layer coordinate, respectively. A_k denotes the z_k-domain at the kth layer and θ_k the orientation with respect to the global x-axis. Stress, strain and displacement components along the global triorthogonal cartesian system are indifferently denoted by subscripts 1, 2, 3 or x, y, z.

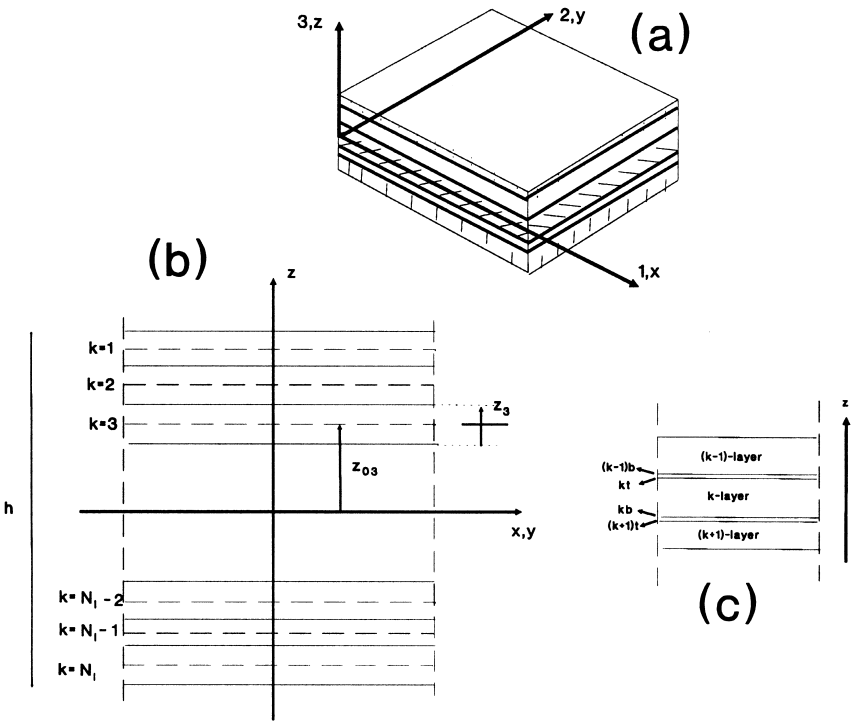

Fig. 1. Geometry and notation. (a) Multilayered plate; (b) notation along thickness coordinate; (c) kth interface.

According to the von Kármán large deflection approximations, the strain components ϵ_{ij} ($i, j = 1, 2, 3$; as in the Reissner–Mindlin model, the normal strain component ϵ_{33} is disregarded) are related to the displacement components u_i ($i = 1, 2, 3$) as in the following:

$$\begin{aligned}
&\{\epsilon^{\mathrm{p}}\} = \{\epsilon^{\mathrm{p}}_{\mathrm{l}}\} + \{\epsilon^{\mathrm{p}}_{\mathrm{nl}}\} = ([B^{\mathrm{p}}_{\mathrm{l}}] + [B^{\mathrm{p}}_{\mathrm{nl}}])\{u\}, \quad \{\epsilon^{\mathrm{n}}\} = [B^{\mathrm{n}}]\{u\},\\
&\delta\{\epsilon^{\mathrm{p}}\} = \delta\{\epsilon^{\mathrm{p}}_{\mathrm{l}}\} + \delta\{\epsilon^{\mathrm{p}}_{\mathrm{nl}}\} = ([B^{\mathrm{p}}_{\mathrm{l}}] + 2[B^{\mathrm{p}}_{\mathrm{nl}}])\delta\{u\},\\
&\delta\{\epsilon^{\mathrm{n}}\} = [B^{\mathrm{n}}]\delta\{u\},
\end{aligned} \tag{1}$$

where the superscripts "p" and "n" denote in-plane and transverse (out-of-plane) components, while subscripts "l" and "nl" denote linear and non-linear components. The explicit form of the arrays is provided in Appendix A. The matrix notation has been extensively used in this paper to concisely handle the governing equations. The first variation (denoted by δ) of the strain has been also quoted in Eq. (1).

In order to meet the proposal of the mechanical model presented in the next subsection, both stiffness coefficients C_{ij} ($i, j = 1, 2, 6$) and compliance coefficients S_{ij} ($i, j = 4, 5$) are used in the following form of Hooke's law:

$$\{\sigma^{\mathrm{p}}\}_k = [C_{\mathrm{pp}}]_k\{\epsilon^{\mathrm{p}}\}_k, \quad \{\epsilon^{\mathrm{n}}\}_k = [S_{\mathrm{nn}}]_k\{\sigma^{\mathrm{n}}\}_k, \tag{2}$$

$\{\sigma^{\mathrm{p}}\}$ and $\{\sigma^{\mathrm{n}}\}$ are the in-plane and out-of-plane stress components, respectively. The explicit form of the arrays is provided in Appendix A.

2.2. Displacement field

In order to include the zig-zag effects, two zig-zag terms are added to the standard Reissner–Mindlin displacement model, as shown by Murakami in Ref. [33]:

$$\left.\begin{aligned}
u^k_1(x,y,z,) &= U^0_1(x,y) + \tfrac{h}{2}\,\zeta U^1_1(x,y) + \zeta_k(-1)^k D_1(x,y)\\
u^k_2(x,y,z) &= U^0_2(x,y) + \tfrac{h}{2}\,\zeta u^1_2(x,y) + \zeta_k(-1)^k D_2(x,y)\\
u^k_3(x,y,z) &= U^0_3(x,y)
\end{aligned}\right\}$$

$$\{u\}_k = [E_{\mathrm{u}}]_k\{X_{\mathrm{u}}\}. \tag{3}$$

U^0_1, U^0_2 and U^0_3 are the displacement components of a point on the reference surface Ω of the plate. U^1_1 and U^1_2 denote the rotations of the normal to the reference surface in the planes x–z and y–z, respectively. $\zeta_k(-1)^k D_1$ and $\zeta_k(-1)^k D_2$ are the zig-zag terms; these terms have the goal of reproducing the discontinuity of the first derivative along z at each layer-interface, see Fig. 2(a). The introduced matrices are written in the Appendix.

2.3. Transverse stress field

The order of the z expansion for the transverse stresses $\{\sigma^{\mathrm{n}}\}$ is established to be quadratic at each kth layer, see Fig. 2(b). The assumed transverse stress

model is [33]:

$$\left.\begin{aligned}\sigma^k_{13}(x,y,z) &= \sigma^{k\mathrm{t}}_{13}(x,y)F_0(z_k) + F_1(z_k)R^k_{13}(x,y) + \sigma^{k\mathrm{b}}_{13}(x,y)F_2(z_k)\\ \sigma^k_{23}(x,y,z) &= \sigma^{k\mathrm{t}}_{23}(x,y)F_0(z_k) + F_1(z_k)R^k_{23}(x,y) + \sigma^{k\mathrm{b}}_{23}(x,y)F_2(z_k)\end{aligned}\right\}\sigma^{\mathrm{n}}\}_k = [E_\sigma]_k\{X_\sigma\}_k. \tag{4}$$

Notice that the model of Eq. (4) uses six k-dependent functions: the two stresses resultants $R^k_{13}(x, y) = \int_{A_k}\sigma^k_{13}(x, y)\,\mathrm{d}z$, $R^k_{23}(x, y) = \int_{A_k}\sigma^k_{23}(x, y)\,\mathrm{d}z$ and the four interface transverse stress values at the top and the bottom of the kth layer (denoted by $\sigma^{k\mathrm{t}}_{13}$, $\sigma^{k\mathrm{t}}_{23}$ and $\sigma^{k\mathrm{b}}_{13}$, $\sigma^{k\mathrm{b}}_{23}$, respectively). Furthermore $F_0 = -1/4 + \zeta_k/2 + 3/4\zeta^2_k$, $F_1 = 3(1-\zeta^2_k)/2\,h_k$, $F_2 = -1/4 - \zeta_k/2 + 3/4\zeta^2_k$. If the equilibria conditions at each interface have to be fulfilled, then the following set of boundary conditions must be linked to the introduced stress unknowns:

(a) layer-interfaces

$$\sigma^{k\mathrm{t}}_{i3} = \sigma^{(k-1)\mathrm{b}}_{i3}, \qquad i = 1,2, \quad k = 2, N_\mathrm{l}$$
$$\sigma^{k\mathrm{b}}_{i3} = \sigma^{(k+1)\mathrm{t}}_{i3}, \qquad i = 1,2, \quad k = 1, N_\mathrm{l}$$

(b) top/bottom of plate

$$4\sigma^{N_\mathrm{l}\mathrm{b}}_{i3} = \bar{\sigma}^{\mathrm{b}}_{i3}, \qquad i = 1,2.$$
$$\sigma^{1\mathrm{t}}_{i3} = \bar{\sigma}^{\mathrm{t}}_{i3}, \qquad i = 1,2. \tag{5}$$

The bar denotes imposed transverse shear stresses. Thus, *the assumed transverse stresses model is capable of fulfilling both interlaminar equilibria and the imposed transverse stress conditions at the top/bottom of the plate*.

2.4. Constitutive equations for the transverse stress unknowns

In order to eliminate the stress unknowns a $\{X_\sigma\}$ reference is made to the method described in Refs [2, 32], where some of the original ideas presented by Reissner [36] were used. A short description follows. Firstly, the following equality is written between transverse shear strains coming from Eq. (1), (subscript G as geometrical) and those from Eq. (2) (subscript H as Hooke),

$$\{\epsilon^{\mathrm{n}}_{\mathrm{G}}\}_k - \{\epsilon^{\mathrm{n}}_{\mathrm{H}}\}_k = 0. \tag{6}$$

By multiplying Eq. (6) with the introduced stress model, Eq. (4) (subscript M as model, to distinguish them from those coming from Hooke's law), then the following weak form equations can be written for each layer:

$$\int_{A_k}\{\delta\sigma^{\mathrm{n}}_{\mathrm{M}}\}^{\mathrm{T}}(\{\epsilon^{\mathrm{n}}_{\mathrm{G}}\}_k - \{\epsilon^{\mathrm{n}}_{\mathrm{H}}\}_k)\,\mathrm{d}z = 0, \quad k = 1, N_\mathrm{l}, \tag{7}$$

where superscript "T" denotes the transposition of arrays. From these, the constitutive equations of the kth lamina for the transverse stresses can be obtained in a form consistent to the assumed models in Eqs. (3) and (4). In fact, upon substitution of these models, Eq. (7) leads to the following set of variational equations:

$$\{\delta X_\sigma\}^{\mathrm{T}}_k([H_\mathrm{u}]_k\{X_\mathrm{u}\} - [H_\sigma]_k\{X_\sigma\}_k) = 0, \quad k = 1, N_\mathrm{l}, \tag{8}$$

where

$$[H_\mathrm{u}]_k = \int_{A_k}[E_\sigma]^{\mathrm{T}}([B_\mathrm{n}]_k[E_\mathrm{u}]_k)\,\mathrm{d}z,$$
$$[H_\sigma]_k = \int_{A_k}[E_\sigma]^{\mathrm{T}}_k[S_{\mathrm{nn}}]_k[E_\sigma]_k\,\mathrm{d}z. \tag{9}$$

The matrix $[H_\sigma]_k$ is symmetric and non-singular, while $[H_\mathrm{u}]_k$ is singular and non-symmetric; these matrices were explicitly written in Ref. [32]. In order to impose the boundary conditions in Eq. (5), it is convenient to obtain the constitutive equations at a multilayered level. This was shown in detail in Ref. [32]. As a result the following constitutive equations are written for each layer between the introduced stress and displacement unknowns:

$$\{X_\sigma\}_k = [C_\mathrm{u}]_k\{X_\mathrm{u}\} + \{\bar{P}^{\mathrm{tb}}\}. \tag{10}$$

Details on the method used to build the matrix $[C_\mathrm{u}]_k$ can be read in Ref. [32]. $\{\bar{P}^{\mathrm{tb}}\}$ is a load vector coming from the imposed transverse shear stress in Eq. (5). In the following it is assumed that $\{\bar{P}^{\mathrm{tb}}\} = 0$.

3. Governing equations

3.1. Finite element approximation on Ω

In the previous section an approximated model along the thickness coordinate has been assumed for the unknown functions $\{u\}$ and $\{\sigma^{\mathrm{n}}\}$. In order to obtain numerical solutions for various geometrical–mechanical boundary conditions and laminated layouts, further approximations must be introduced on the plate domain Ω. Herein, reference is made to the finite element method (FEM). In such a context Ω is subdivided in a certain number of elements. Then assumptions are made for the behaviour of the unknown vector $\{X_\mathrm{u}\}$ in each element domain. As the 2D model

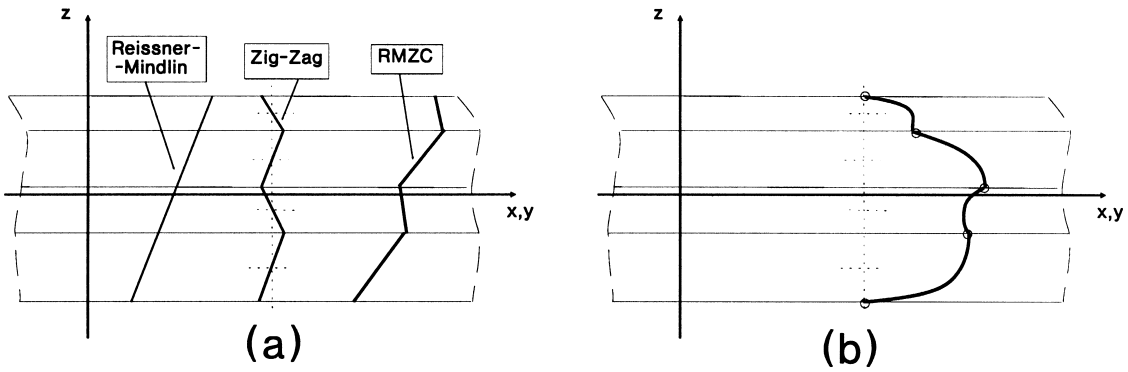

Fig. 2. Assumed C_z^0 models. (a) In-plane displacements u_1 and u_2; (b) transverse shear stresses σ_{13} and σ_{23}.

has been formulated with C^0 continuity, an isoparametric description can be referred. For example, for the unknown U_1^0 one has:

$$U_1^0(x,y)=\sum_i^{N_n} N_i(\xi,\eta)Q_{U_1^0}^i \quad \text{or} \quad U_1^0(x,y)=\{n\}^T\{Q_{U_1^0}\}, \tag{11}$$

where $N_i(\xi,\eta)$ are N_n shape functions (N_n is the number of the nodes) defined in the natural plane ξ, η, see Refs [27,29]. In the isoparametric formulation, the same shape functions are used for the different unknowns, so that the unknown vector is written as:

$$\{X_u\}=[N]\{Q_u\}. \tag{12}$$

$[N]$ is a diagonal matrix whose elements are the shape functions $N_i(\xi,\eta)$, while

$$\{Q_u\}=(\{Q_{U_1^0}\},\{Q_{U_2^0}\},\{Q_{U_3^0}\},\{Q_{U_1^1}\},\{Q_{U_2^1}\},\{Q_{D_1}\},\{Q_{D_2}\})$$

is the vector of the $7\times N_n$ unknowns at element level.

3.2. Equilibrium equations

Let us consider a multilayered plate of volume V subjected to external mechanical loads. In the static case the principle of virtual displacement states:

$$\delta L_i=\delta L_m+\delta L_e \tag{13}$$

where δL_i is the virtual variation of internal work, δL_e is the virtual variation of the work done by the applied external loads and δL_m is the virtual variation of the work done by inertial forces. The variation of the internal work can be split into in-plane and out-of-plane contributions:

$$\delta L_i=\delta L_l^p+\delta L_{nl}^p+\delta L_l^n. \tag{14}$$

The in-plane or bending contribution has been split into a linear and non-linear part. With the adopted notations and approximations, introduced step by step, one has:

$$\begin{aligned}\delta L_l^p &= \int_V \delta\{\epsilon_l^p\}^T\{\sigma_l^p\}_k\,dV\\ &= \int_V \delta([B_l^p]\{u\}_k)^T([C_{pp}]_k[B_l^p]\{u\}_k)dV\\ &= \int_V \delta([B_l^p]([E_u]_k\{X_u\}))^T([C_{pp}]_k[B_l^p]([E_u]_k\{X_u\}))\,dV\\ &= \int_V \delta([B_l^p]([E_u]_k([N]\{Q_u\})))^T\\ &\quad([C_{pp}]_k[B_l^p]([E_u]_k([N]\{Q_u\})))\,dV\\ &= \delta\{Q_u\}^T[K_l^p]\{Q_u\},\end{aligned} \tag{15}$$

where $[K_l^0]$ is the stiffness matrix related to the linear contribution of the bending deformations. At the same way the shear contribution reads:

$$\begin{aligned}\delta L_l^n &= \int_V \delta\{\epsilon^n\}^T\{\sigma_l^n\}_k\,dV\\ &= \int_V \delta([B^n]\{u\}_k)^T([E_\sigma]_k\{X_\sigma\}_k)\,dV\\ &= \int_V \delta([B^n]([E_u]_k\{X_u\}))^T([E_\sigma]_k([C_u]_k\{X_u\}))\,dV\\ &= \int_V \delta([B^n]([E_u]_k([N]\{Q_u\})))^T([E_\sigma]_k([C_u]_k([N]\{Q_u\})))\,dV\\ &= \delta\{Q_u\}^T[K^n]\{Q_u\},\end{aligned} \tag{16}$$

where $[K^n]$ is the shear contribution to the stiffness matrix. Global non-linear stiffness matrices are obtained in a symmetric form by referring to the method proposed in Ref. [37]. According to that the variation of the virtual work related to the non-linear

deformations is written as:

$$\begin{aligned}\delta L_{\mathrm{nl}}^{\mathrm{p}} &= \int_V \Big((\delta\{\epsilon_{\mathrm{l}}^{\mathrm{p}}\}^{\mathrm{T}}\{\sigma_{\mathrm{nl}}^{\mathrm{p}}\} + \frac{1}{2}\delta\{\epsilon_{\mathrm{nl}}^{\mathrm{p}}\}^{\mathrm{T}}\{\sigma_{\mathrm{l}}^{\mathrm{p}}\}_k \\ &\quad + \frac{1}{2}\delta\{\epsilon_{\mathrm{l}}^{\mathrm{p}}\}^{\mathrm{T}}\{\sigma_{\mathrm{l}}^{\mathrm{p}}\}_k + \delta\{\epsilon_{\mathrm{nl}}^{\mathrm{p}}\}^{\mathrm{T}}\{\sigma_{\mathrm{nl}}^{\mathrm{p}}\}_k \Big)\,\mathrm{d}V \\ &= \int_V \delta([B_{\mathrm{l}}^{\mathrm{p}}]([E_{\mathrm{u}}]_k([N]\{Q_{\mathrm{u}}\})))^{\mathrm{T}} \\ &\quad \times ([C_{\mathrm{pp}}]_k[B_{\mathrm{nl}}^{\mathrm{p}}]([E_{\mathrm{u}}]_k([N]\{Q_{\mathrm{u}}\})))\,\mathrm{d}V \\ &\quad + \frac{1}{2}\int_V \delta([B_{\mathrm{nl}}^{\mathrm{p}}]([E_{\mathrm{u}}]_k([N]\{Q_{\mathrm{u}}\})))^{\mathrm{T}} \\ &\quad \times ([C_{\mathrm{pp}}]_k[B_{\mathrm{l}}^{\mathrm{p}}]([E_{\mathrm{u}}]_k([N]\{Q_{\mathrm{u}}\})))\,\mathrm{d}V \\ &\quad + \frac{1}{2}\int_V \delta([B_{\mathrm{nl}}^{\mathrm{p}}]([E_{\mathrm{u}}]_k([N]\{Q_{\mathrm{u}}\})))^{\mathrm{T}}\{\sigma_{\mathrm{l}}^{\mathrm{p}}\}_k))\,\mathrm{d}V \\ &\quad + \int_V \delta([B_{\mathrm{nl}}^{\mathrm{p}}]([E_{\mathrm{u}}]_k([N]\{Q_{\mathrm{u}}\})))^{\mathrm{T}} \\ &\quad \times ([C_{\mathrm{pp}}]_k[B_{\mathrm{nl}}^{\mathrm{p}}]([E_{\mathrm{u}}]_k([N]\{Q_{\mathrm{u}}\})))\,\mathrm{d}V \\ &= \frac{1}{2}\delta\{Q_{\mathrm{u}}\}^{\mathrm{T}}([K_{\mathrm{lnl}}^{\mathrm{p}}] + [K_{\mathrm{nll}}^{\mathrm{p}}] + [K_{\sigma_{\mathrm{l}}}^{\mathrm{p}}] + [K_{\mathrm{nlnl}}^{\mathrm{p}}])\{Q_{\mathrm{u}}\}, \quad (17)\end{aligned}$$

where the initial stress or geometric stiffness matrix $[K_{\sigma_{\mathrm{l}}}^{\mathrm{p}}]$ related to the linear part of the in-plane stresses has been introduced. The factor 1/2 underlines that the exception made for the initial stress matrix, the non-linear part of the secant matrix, can be obtained as one half of the corresponding non-linear part of the tangent matrix, see the next subsection. Explicit forms of the derived matrices can be found in Refs [34, 35]. The work done by inertia forces is given by:

$$\begin{aligned}\delta L_{\mathrm{m}} &= -\int_V \rho_k\{\delta u\}_k^{\mathrm{T}}\{\ddot{u}\}_k\,\mathrm{d}V \\ &= -\int_V \rho_k\{\delta X_{\mathrm{u}}\}_k^{\mathrm{T}}[E_{\mathrm{u}}]_k^{\mathrm{T}} > [E_{\mathrm{u}}]_k\{\ddot{X}_{\mathrm{u}}\}_k\,\mathrm{d}V, \quad (18)\end{aligned}$$

where ρ_k is the mass-density of the kth layer.

The variation of external work given by distributed pressure and/or point loads can be written as:

$$\delta L_{\mathrm{e}} = \delta\{Q_{\mathrm{u}}\}^{\mathrm{T}}\{P(t)\}, \quad (19)$$

where $\{P(t)\}$ is the load vector equivalent, in the finite element sense, to the applied time-dependent loads. finally, from Eq. (13), the approximate form of equilibrium reads:

$$[M]\{\ddot{Q}_{\mathrm{u}}\} + [K_{\mathrm{S}}]\{Q_{\mathrm{u}}\} = \{P(t)\}, \quad (20)$$

where the secant stiffness matrix is:

$$\begin{aligned}[K_{\mathrm{S}}] &= [K_{\mathrm{l}}^{\mathrm{p}}] + [K_{\mathrm{l}}^{\mathrm{n}}] + \frac{1}{2}[K_{\mathrm{nl}}^{\mathrm{p}}] + \frac{1}{2}[K_{\sigma_{\mathrm{l}}}], \\ &\quad \text{with} \quad [K_{\mathrm{nl}}^{\mathrm{p}}] = [K_{\mathrm{lnl}}^{\mathrm{p}}] + [K_{\mathrm{nll}}^{\mathrm{p}}] + [Kp_{\mathrm{nlnl}}]. \quad (21)\end{aligned}$$

The above equations have been written at element level; they take the same form when written at structure level. In this case, the element arrays are assembled with the usual FEM techniques.

3.2.1. Structural damping.

Many possibilities are available to introduce structural damping in the approximate model presented, see Ref. [29] as an example. In this paper, we use Rayleigh damping to build the damping matrix from the mass and stiffness matrices at structure level

$$[D] = \alpha[M] + \beta[K_{\mathrm{l}}], \quad (22)$$

where α and β are two constants and the linear contribution to the stiffness matrix has been used. Hence, the dynamic equilibrium at time t reads:

$$[M]\{\ddot{Q}_{\mathrm{u}}\} + [D]\{\dot{Q}_{\mathrm{u}}\} + [K_{\mathrm{S}}(\{Q_{\mathrm{u}}\})]\{Q_{\mathrm{u}}\} = \{P(t)\}. \quad (23)$$

3.3. Static and dynamic solution

If the static case is considered, Eq. (23) reduces to

$$[K_{\mathrm{S}}(\{Q_{\mathrm{u}}\})]\{Q_{\mathrm{u}}\} = \lambda\{P_{\mathrm{ref}}\}. \quad (24)$$

The applied load vector is supposed to be displacement-independent and to be proportionally increased by means of the load parameter λ from the initial reference configuration $\{P_{\mathrm{ref}}\}$.

A standard solution scheme can be obtained by following the straightforward application of the Newton–Raphson method between the initial equilibrium state i and the unknown state $i+1$ (in the neighborhood of i). Linearization at the known state i yields (Δ denotes finite variations between the two states i and $i+1$):

$$[K_{\mathrm{T}}(\{Q_{\mathrm{u}}\}_i)]\Delta\{Q_{\mathrm{u}}\} = \Delta\lambda\{P_{\mathrm{ref}}\} + \{\varphi_{\mathrm{res}}\}, \quad (25)$$

where $\Delta\{Q_{\mathrm{u}}\}$ is the increment of the displacement vector and $\{\varphi_{\mathrm{res}}\} = \lambda_i\{P_{\mathrm{ref}}\} - [K_{\mathrm{S}}(\{Q_{\mathrm{u}}\}_i)]\{Q_{\mathrm{u}}\}_i$ is the residual vector of the unbalanced nodal forces. $[K_{\mathrm{T}}(\{Q_{\mathrm{u}}\})]$ is the tangent stiffness matrix that arises from the linearization as the second variation of the internal work:

$$\begin{aligned}\Delta(\delta L_{\mathrm{i}}) &= \Delta\Big(\int_V \delta\{\epsilon\}^{\mathrm{T}}\{\sigma\}\,\mathrm{d}V \\ &\quad = \int_V (\Delta\delta\{\epsilon\}^{\mathrm{T}}\{\sigma\} + \delta\{\epsilon\}^{\mathrm{T}}\Delta\{\sigma\}\Big)\,\mathrm{d}V \\ &= \delta\{Q_{\mathrm{u}}\}^{\mathrm{T}}([K_{\mathrm{l}}^{\mathrm{p}}] + [K_{\mathrm{l}}^{\mathrm{n}}] + [K_{\mathrm{nl}}^{\mathrm{p}}] + [K_{\sigma}^{\mathrm{p}}])\Delta\{Q_{\mathrm{u}}\} \\ &= \delta\{Q_{\mathrm{u}}\}^{\mathrm{T}}[K_{\mathrm{T}}(\{Q_{\mathrm{u}}\})]\Delta\{Q_{\mathrm{u}}\}. \quad (26)\end{aligned}$$

Then

$$[K_{\mathrm{T}}] = [K_{\mathrm{l}}^{\mathrm{p}}] + [K_{\mathrm{l}}^{\mathrm{n}}] + [K_{\mathrm{nl}}^{\mathrm{p}}] + [K_{\sigma}^{\mathrm{p}}], \quad (27)$$

with the same matrices as found in Eq. (20). Note that the initial stress matrix $[K_{\sigma}^{\mathrm{p}}]$ now refers to both the linear and non-linear part of the in-plane stresses $\{\sigma^{\mathrm{p}}\}$.

Since the load level λ is treated as a variable, an extra governing equation is required in the form of a constraint relationship $c(\{\Delta Q_{\mathrm{u}}\}, \Delta\lambda) = 0$. Finally, the

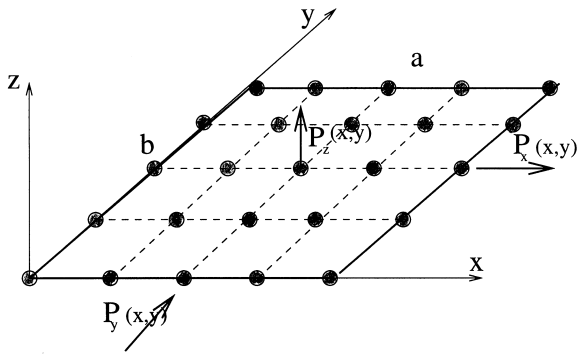

Fig. 3. Notation used for the applied loadings in the finite element model.

following complete system follows:

$$\begin{cases} [K_T(\{Q_u\})]\{\Delta Q_u\} = \Delta\lambda\{P_{ref}\} - \{\varphi_{res}\} \\ c(\{\Delta Q_u\}, \Delta\lambda) = 0 \end{cases}. \tag{28}$$

Several forms of the constraint equation have been proposed in the FEM literature. Reviews can be found in Ref. [38]. In the following numerical investigations we will use a constant load increment in each load-step. The Newmark time integration scheme [28, 39] widely used in structural dynamics, particularly for non-linear problems where modal methods are no more applicable, is here employed. The equation of motion at time $t + \Delta t$ is then:

$$[M]\{\ddot{Q}_u\}_{i+1} + [D]\{\dot{Q}_u\}_{i+1} + [K_S(\{Q_u\}_{i+1})]\{Q_u\}_{i+1} = \{P\}_{i+1}. \tag{29}$$

The Newmark approximations for the displacements and velocities within the time step Δt are introduced, leading to a standard predictor-multi-corrector scheme. The values $\tau = 1/4$ and $\gamma = 1/2$ are employed for the related constants [29].

4. Results and discussion

In order to compare the CLT, FSDT and RMZC approximations, as well as the linear and non-linear analyses, several problems have been analysed. The employed finite element technique easily permits to change loading conditions and lamination schemes.

4.1. Data description

Square plates with different values of the thickness ratio a/h are investigated (a and h are length and plate thickness, respectively). Nine-node parabolic Lagrangian type elements have been used [27] and two regular meshes of 2×2 and 4×4 elements to discretize quarter and full plates, respectively. The used mechanical properties of the lamina, with usual notations [40], are: E_l = variable, $E_t = 1$, $G_{lt} = 0.5$, $G_{tt} = 0.35$, $\nu_{lt} = \nu_{tt} = 0.3$. Consistent units for both mechanical and geometrical characteristics are intended everywhere. The considered cross-ply, symmetrically and unsymmetrically, laminated layouts are made of laminae of equal thickness. Boundary conditions are herein restricted to the simply-supported type. For a quarter of the plate we refer to: $x = 0$: $U_1^0 = U_1^1 = U_3^0 = 0$; $x = a/2$: $U_1^0 = U_1^1 = 0$; $y = 0$: $U_2^0 = U_1^2 = U_3^0 = 0$; $y = a/2$: $U_2^0 = U_2^1 = 0$. While for the full meshed plate we refer to: $x = 0$, a and $y = 0$, a: $U_3^0 = 0$; in $x = 0$: $U_1 = U_2 = 0$. The plates are bended by transverse point loads and/or by in-plane loads along the y-direction. See Fig. 3 for notations. Both harmonic and step loading conditions will be considered, and damped vibration in both cases of transient and steady-state solutions are analysed. The CLT results are obtained through the application of a penalty technique to the shear correction factor; the value $\chi = 10^3$ has been used. Where not declared, FSDT results refer to the value $\chi = 1$. The transverse displacement and velocity at the plate centre will be plotted in all the analyses. Additional data of the presented problem will be directly mentioned in the captions of the figures. Each caption will describe the analysis and quote all used data, i.e. geometry, mesh, layout, reference loading conditions (the direction of each load is denoted by a subscript, while the coordinate of the point where they are applied is denoted in parenthesis), characteristics of the dynamic excitation (A_m is the amplitude, ω_e is the circular frequency of the applied harmonic load, while t_i and t_f denote the instants in which a step-load is applied and removed, respectively) and damping parameters.

4.2. Some preliminary results on linear dynamics and non-linear statics

Some keypoints of the used model are briefly outlined in the following. Table 1 compares the present analysis to the other HSDT solution [26] and to the 3D solution [41]. Symmetrically and unsymmetrically cross-ply laminated thick plates with different values of the orthotropic ratios E_l/E_t are investigated. The RMZC analysis very much improves the FSDT results, particularly when higher orthotropic ratios are considered. A reasonable agreement has been acquired with the quoted references, particularly for the symmetrically laminated cases. As is well known [1], the use of a shear correction factor in the FSDT theory, has no physical background. Low values of it can lead to plates more deformable compared with the 3D analysis. In particular, the value $\chi = 5/6$ corresponds to a parabolic distribution of the transverse shear stresses if, and only if, one isotropic layer is considered. In

Table 1
Comparisons among different theories on the not dimensionalized, free circular frequencies $\bar{\omega}=\omega h(\sqrt{\rho}/E_t)$ (thick plate $a = 5$, $h = 1$; mesh 2×2; cross-ply)

N_l	E_l	Present analysis				HSDT	3D
		RMZC —	FSDT $\chi = 1$	FSDT $\chi = 5/6$	CLT $\chi = 1000$	[26]	[41]
4	40	0.4283	0.4406	0.4175	0.6647	0.3899	0.3887
4	3	0.2521	0.2543	0.2498	0.2813	0.2495	0.2493
5	40	0.4222	0.4410	0.4166	0.7302	0.4121	0.4102
5	3	0.2544	0.2543	0.2529	0.2868	0.2528	0.2529
—	1*	0.2113	0.2143	0.2113	0.2316	—	—

* Isotropic case.

fact, in the isotropic case (shear moduli are calculated according to the value $v = 0.3$) one finds out that the RMZC model (which assumes a parabolic distribution of the transverse shear stresses) coincides to the corresponding FSDT result.

The possibilities of the presented RMZC model to approach the zig-zag form of the displacement field along the thickness are shown in Fig. 4. Comparisons to the CLT and FSDT solutions are presented. These theories, as well as the HSDT in Ref. [26], even though they are quite acceptable for the analysis of global characteristics (maximum deflections, natural frequencies, etc.), they can lead to significant errors in the evaluation of the distribution of stresses and displacements along the thickness of thick plates. An exhaustive discussion on the performance of the RMZC model in linear static analysis can be found in Ref. [32].

The capability of the used von Kármán-type non-linear model to approach large displacements behaviour in the static postbuckling range, is briefly outlined in Fig. 5. The RMZC, FSDT and CLT results are compared. The plotted load factor scales the reference loading configuration described in the caption. A transverse distribution load P_z has been applied at the centre of the plate, in order to simulate geometrical imperfections and to compute the postbuckling range. A more complete analysis on this topic, including details on the C_z^0 requirements in the large deflection and postbuckling field, can be found in Ref. [34].

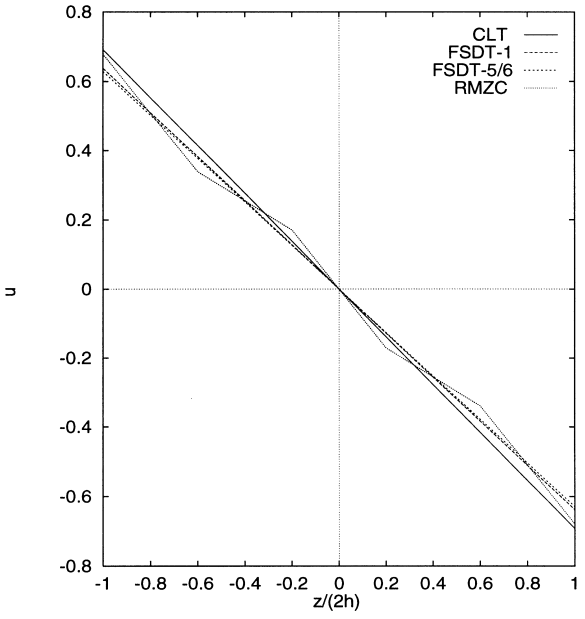

Fig. 4. Distribution of the in-plane displacement $u_1(0, b/2, z)$ along the plate thickness. Comparisons among different theories ($a = 5$, $h = 1$; mesh 2×2; $0°/90°/0°/90°/0°$, $E_l = 40$. $P_z(2.5, 2.5) = 1$).

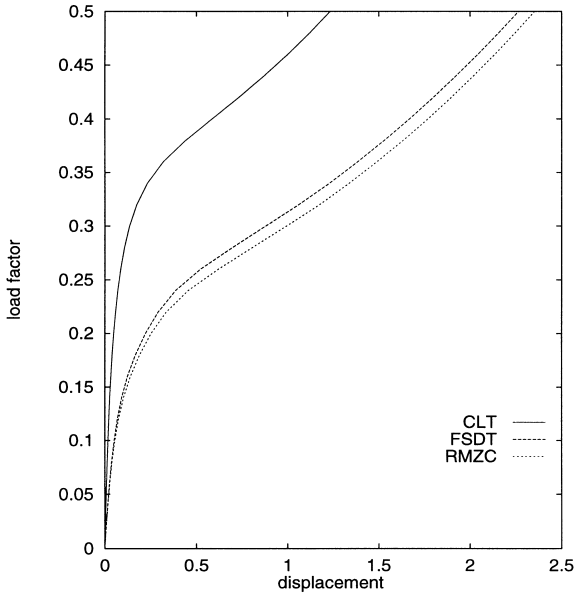

Fig. 5. Postbuckling of a compressed plate. Comparisons among different theories ($a = 10$, $h = 1$; mesh 4×4. $0°/90°/0°/90°/0°$, $E_l = 40$. Reference loadings: $P_y(0, 10) = P_y(2.5, 10) = P_y(5, 10) = P_y(7.5, 10) = P_y(10, 10) = -2$, $P_z(5, 5) = 0.1$).

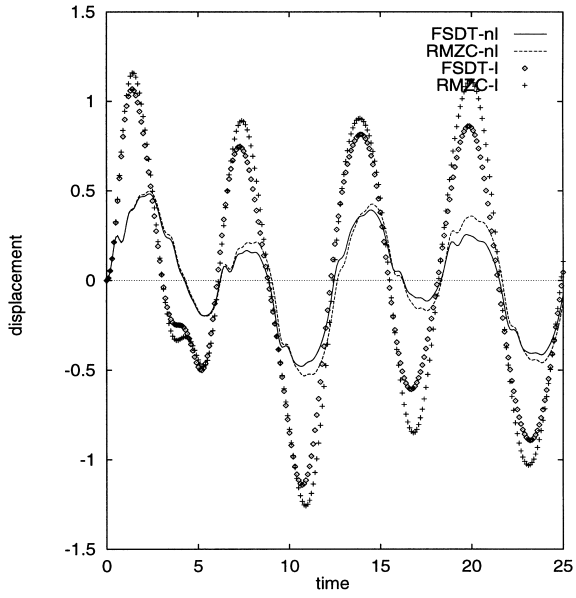

Fig. 6. Transient of damped forced harmonic vibration. Comparison between the RMZC and FSDT results in both linear and non-linear analysis ($a = 5$, $h = 1$; mesh 2×2; $0°/90°/0°/90°/0°$, $E_1 = 40$; $P_z(2.5, 2.5) = 1$, $P_z(1.25, 2.5) = P_z(2.5, 1.25) = P_z(1.25, 1.25) = 0.5$. $A_m = 1$, $\omega_e = 1$; $\alpha = 0.035$, $\beta = 0.034$).

4.3. Symmetrically and unsymmetrically laminated plates subjected to in-plane and out-of-plane dynamic loadings

The transient forced vibration of cross-ply laminated thick plates is investigated in Fig. 6. The FSDT and RMZC results for both linear and non-linear solutions are compared. The linear theory leads to large errors even though the maximum deflection remains in the same order of magnitude as the plate thickness. Higher modes are evident in the non-linear analysis. The FSDT overestimates the deflection with respect to the RMZC analysis (the frequency of the oscillations cannot be different to that of the applied harmonic forces).

Linear and non-linear results for both small and moderate amplitude vibrations are compared in Fig. 7. A cross-ply unsymmetrically laminated thick plate is considered. The RMZC results have been plotted in the case of harmonic forced vibrations. Linear and non-linear results agree very well in the case of small amplitude, just some differences can be noted in the maximum amplitudes. Very different results are obtained in the case of moderate amplitude vibrations. One notices that in this case the steady-state solution is not yet reached for the considered integration time. The presence of higher modes in the non-linear cases has to be remarked.

In order to simulate the non-linear free response of laminated plates, a load step function has been applied. Results are quoted in Figs. 8 and 9 for linear and non-linear analysis, respectively. A symmetrically laminated, thick plate has been investigated and the CLT, FSDT and RMZC are compared. Owing to the presence of damping, the oscillations tend to the static solutions, which in these cases coincide with the undeformed configurations. The initial oscillations in the linear case have a very large amplitude. The CLT underestimates the deflections greatly, furthermore it is not affected by higher modes. Very small deflections are obtained in the non-linear case. Higher modes are faster damped compared with the linear case. The frequency of the transient vibration increases in the non-linear cases. Furthermore, it depends on the used theory. In particular, the difference between the CLT and the other two theories becomes evident.

To investigate the behaviour of the three theories in thin plate analysis, the same problem as in Fig. 8 has been treated in Fig. 10 for the value $h = 0.1$ of the plate thickness. Both the RMZC and FSDT model approach the thin plate theories, furthermore, as found in Refs [32, 34] for the linear and non-linear static analysis, the RMZC and FSDT coincide.

Very usual loading conditions of composites panels are considered in Fig. 11. An unsymmetrically laminated cross-ply plate is subjected to axial load, as in

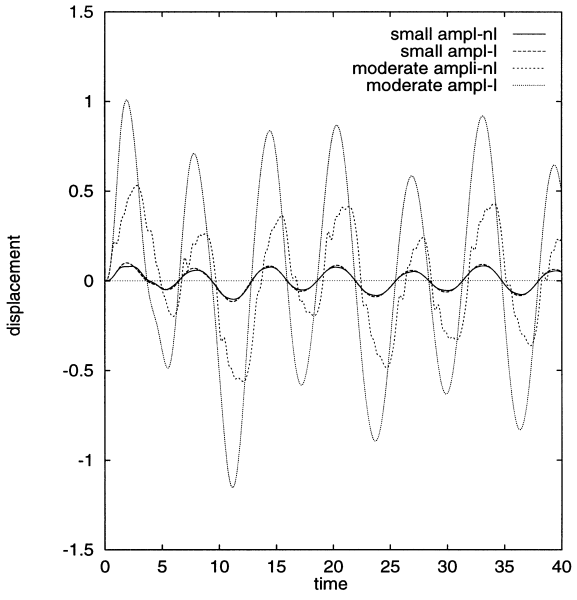

Fig. 7. Small and moderate amplitude forced harmonic vibrations. Comparison of linear and non-linear analysis. The RMZC results ($a = 5$, $h = 1$; mesh 2×2; $0°/90°/0°/90°$, $E_1 = 40$; $P_z(2.5, 2.5) = 1$, $P_z(1.25, 2.5) = P_z(2.5, 1.25) = P_z(1.25, 1.25) = 0.5$; $A_m = 0.1$ (moderate amplitude), $A_m = 0.01$ (small amplitude), $\omega_e = 1$; $\alpha = 0.035$, $\beta = 0.034$).

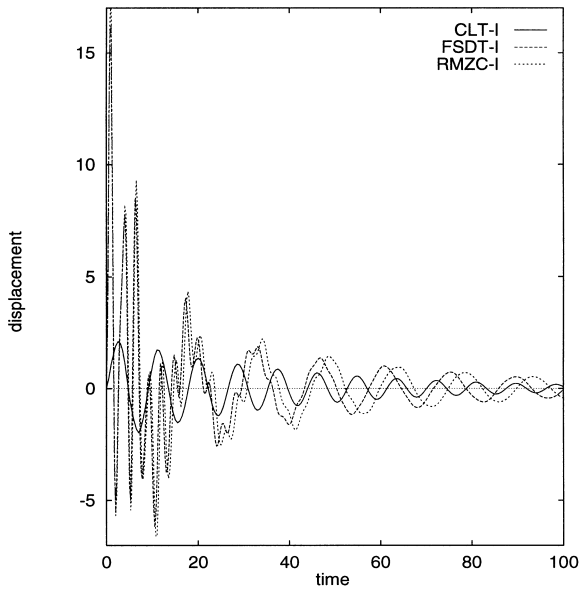

Fig. 8. Transient damped response to step loading. Comparison of different theories. Linear analysis ($a = 5$, $h = 1$; mesh 2×2; $0°/90°/0°/90°/90°$, $E_l = 40$; $P_z(2.5, 2.5) = 1$, $P_z(1.25, 2.5) = P_z(2.5, 1.25) = P_z(1.25, 1.25) = 0.5$; $A_m = 2$, $t_i = 0$, $t_f = 0.5$; $\alpha = 0.035$, $\beta = 0.034$).

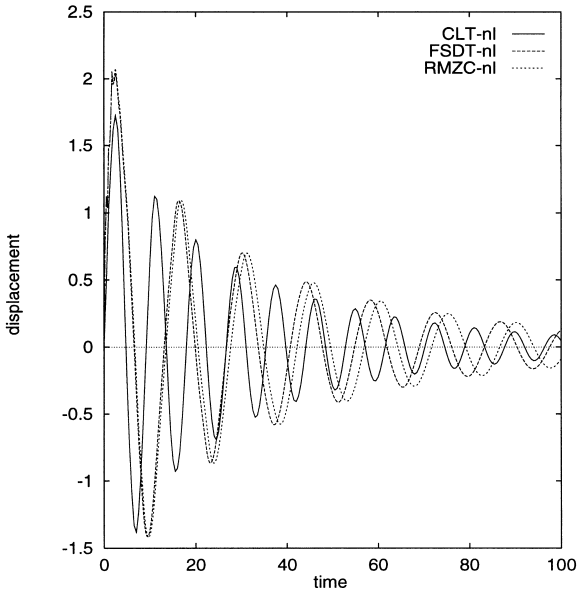

Fig. 9. Transient damped response to step loading. Comparison of different theories. Non-linear analysis ($a = 5$, $h = 1$; mesh 2×2; $0°/90°/0°/90°/90°$, $E_l = 40$; $P_z(2.5, 2.5) = 1$, $P_z(1.25, 2.5) = P_z(2.5, 1.25) = P_z(1.25, 1.25) = 0.5$; $A_m = 2$, $t_i = 0$, $t_f = 0.5$ $\alpha = 0.035$, $\beta = 0.034$).

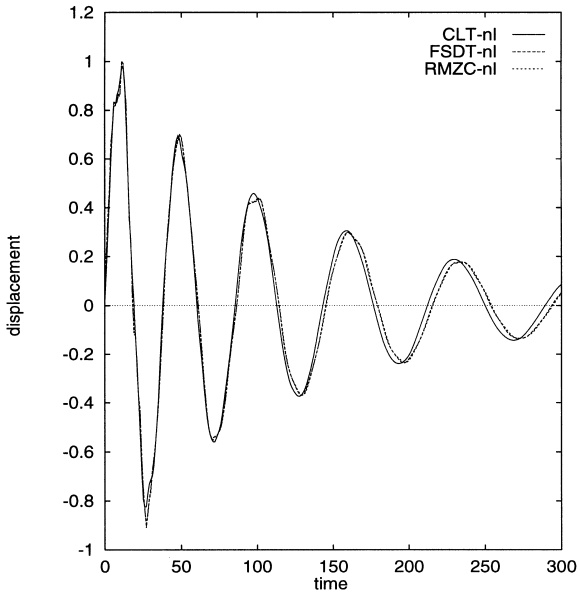

Fig. 10. Comparison of the different theories in thin plate analysis. Transient damped response to step loading. Non-linear results ($a = 5$, $h = 0.1$, mesh 2×2; $0°/90°/0°/90°/90°$, $E_l = 40$; $P_z(2.5, 2.5) = 1$, $P_z(1.25, 2.5) = P_z(2.5, 1.25) = P_z(1.25, 1.25) = 0.5$. $A_m = 0.004$, $t_i = 0$, $t_f = 0.5$; $\alpha = 0.015$, $\beta = 0.014$).

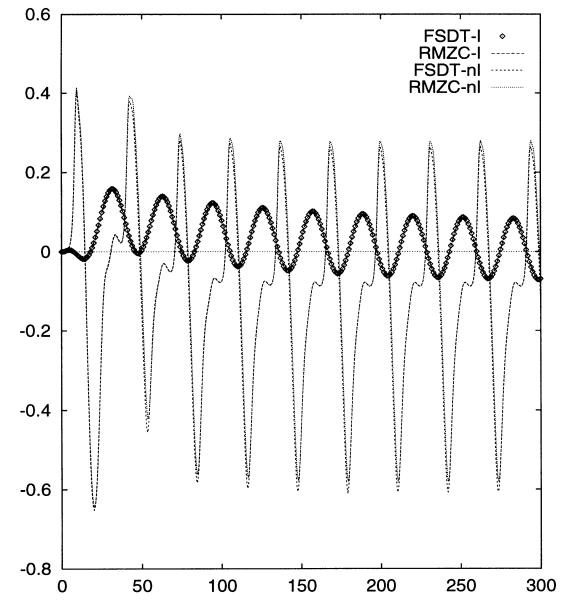

Fig. 11. In-plane damped vibrations of unsymmetrically laminated plates. Comparison between the RMZC and FSDT results in the linear and non-linear cases ($a = 10$, $h = 1$, mesh 4×4; $0°/90°/0°/90°/$, $E_l = 4$; $P_y(0, 10) = P_y(2.5, 10) = P_y(5, 10) = P_y(1.5, 10) = P_y(7.5, 10) = P_y(10, 10) = -2$; $A_m = -1$, $\omega_e = 0.2$; $\alpha = 0.535$, $\beta = 0.534$).

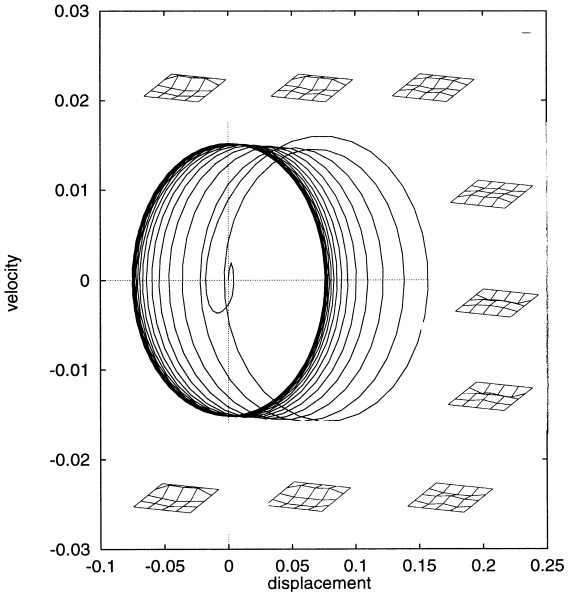

Fig. 12. Phase diagram and deformed plate modes related to the last limit cycle computed. Linear, RMZC case at Fig. 11.

Fig. 4. As the laminate is unsymmetric, transverse deflections arise without any need of imperfections or transverse loadings [17, 43]. The FSDT and RMZC deflections due to harmonic forced vibrations are plotted in both linear and non-linear cases. Owing to the in-plane compression, large deflections are made evident even though low values of the applied loads

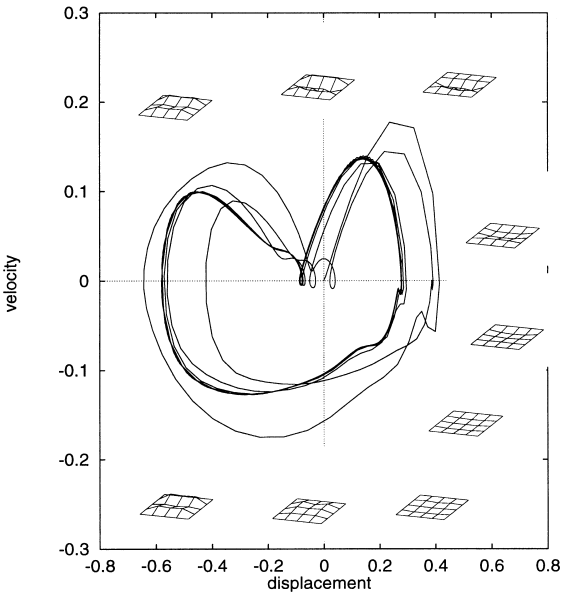

Fig. 13. Phase diagram and deformed plate modes related to the last limit cycle computed. Non-linear, RMZC case at Fig. 11.

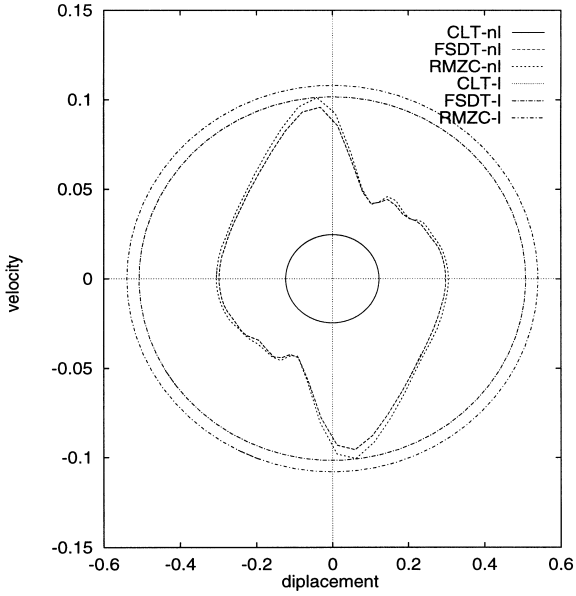

Fig. 14. Phase diagram corresponding to the steady-state solution. Comparison between linear and non-linear analysis for the RMZC, FSDT and CLT results (a = 10, h = 1, mesh 4 × 4; 45°/ − 45°/45°/ − 45°/45°, E_l = 40; P_z(5, 5) = 1; A_m = 3, ω_e = 0.2; α = 0.535, β = 0.534).

are considered. Therefore, in this case, the non-linear analysis leads to deflections larger than those coming from the linear calculations. As in some of the previous analyses, the non-linear results show the presence of higher modes. Furthermore, due to the coupling between membrane and bending strains, the difference between the maximum and minimum amplitude values of the deflections is confirmed [19, 26].

The phase diagrams related to the linear and non-linear analysis of Fig. 11 have been plotted in Figs. 12 and 13. The RMZC results are considered and, in correspondence to the last period, calculated, the sequences of the deformation modes (in clockwise sense) have been drawn. These two plots make evident the different behaviour of linear and non-linear analysis with respect to the deformation modes involved in the deformation process of the considered thick plates. As in the static stability analysis of thick plates [42–46], the difference between the linear and non-linear analyses is also quantitative and qualitative.

The phase diagrams corresponding to the steady-state solutions of a symmetrically laminated angle-ply thick plate have been drawn in Fig. 14. The harmonic forced out-of-plane loading case is considered. The linear solutions overestimate the plate deflections. The RMZC and FSDT solutions include higher modes in the non-linear cases. Owing to the larger anisotropy, the three theories differ more than the cross-ply cases. In correspondence with low values of the displace-

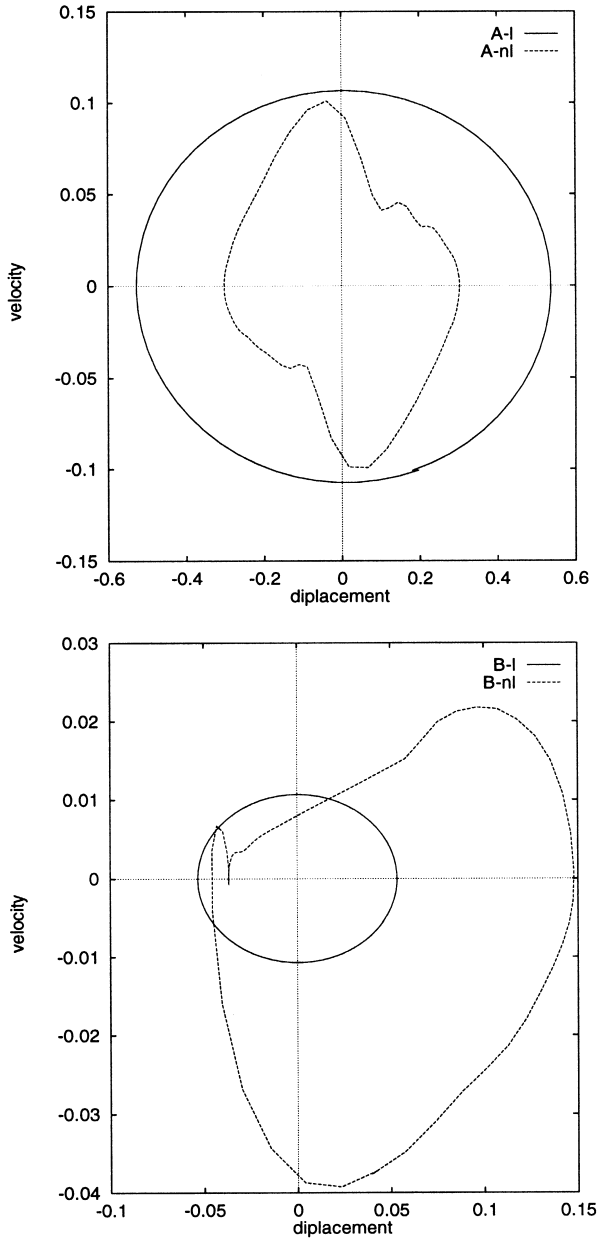

Fig. 15. Phase diagram corresponding to the steady-state solution. Comparison between linear and non-linear analysis for two different loading cases. The RMZC results ($a = 10$, $h = 1$, mesh 4×4; $45°/-45°/45°/-45°$, $E_l = 40$; case A: $P_z(10, 10) = 1$; case B: $P_z(10, 10) = 1$, $P_y(0, 10) = P_y(2.5, 10) = P_y(5,10) = P_y(7.5, 10) = P_y(10, 10) = -2$; $A_m = 3$, $\omega_e = 0.2$, $\phi = 0$; $\alpha = 0.535$, $\beta = 0.534$.

ments, because of energy reasons, the difference between the velocity in the linear and non-linear cases decreases.

Phase diagrams are also plotted in Fig. 15 for an unsymmetrically angle-ply laminated plate. Linear and non-linear solutions in the case of the RMZC analysis are compared for two different loading cases. In case A, only a transverse load is applied at the centre of the plate, while case B adds in-plane loadings. For case A, the linear solution overestimates the plate deflections, while in case B, it should be remarked that the linear solution underestimates the plate deflections in the tension zone but, for the considered case, there is still a zone in the phase diagram where the linear solution overestimates the deflections. That is due to the fact that the in-plane stiffness of the plate depends on: (1) orientations of the load (tension or compression); (2) the level of the loads i.e. of the displacements; and (3) the lamination schemes. Such a unique conclusion cannot be drawn.

5. Concluding remarks

The paper has presented the extension to non-linear dynamic analysis of a 2D model, which, accounting for C_z^0, permits an accurate prediction of the mechanical behaviour of moderately thick, multilayered plates. Approximate governing equations have been written by referring to the finite element technique in conjunction with Newton–Raphson linearization and Newmark time-integration methods. Numerical results have been presented for thick and thin plate geometries, cross-ply and angle-ply layout (symmetric and unsymmetric), as well as in-plane and out-of-plane loading conditions (the damped vibrations caused by harmonic and step loadings force have been treated). Comparisons with linear analysis and both the CLT and FSDT have been made for most of the treated problems. From the conducted analyses the following conclusions can be drawn.

1. The used RMZC models, accounting for an accurate description of both the in-plane displacements and the transverse shear field along the plate thickness, improves the FSDT results in thick plate analysis. Such improvements are more evident in the non-linear case compared with the linear one, furthermore, they are layout-dependent. As in linear and non-linear static analysis, the good performance of FSDTs to analyse the non-linear dynamics of thin plates has been confirmed.
2. With respect to circular frequencies, vibration amplitudes and deformation modes, the non-linear dynamic analysis of thick plates has led to very different results with respect to the linear one. It has been shown that in many cases, the classical lamination models lead to very poor descriptions.
3. The difference among the CLT, FSDT and RMZC models, as well as between non-linear and linear analyses, is very much subordinate to: (1) loading

conditions; (2) geometries; and (3) lamination schemes. In particular, it has been found that the known different behaviour between tension and compression loading cases exhibited by unsymmetrically laminated plates, is very much subordinate to both the type and level of the applied loads.

4. The developed finite element approximation technique is very suitable to treat different geometries, loading types, layouts and boundary conditions. Thus, it can be used for the investigation of the various conditions to which laminated panels are subjected in practice.

Acknowledgements

This work was supported by grants of the German Research Foundation DFG (Deutsche Forschungsgemeinschaft) within the graduate Collegium GKKS (Graduiertenkolleg für Diskretisierungsmethoden für Kontinua und Strömungen).

Appendix A

A.1. Appendix: Explicit form of arrays

A.1.1. Strain-displacement relations

$$\{u\}^{\mathrm{T}} = \{u_1, u_2, u_3\}, \quad \{\epsilon^{\mathrm{p}}\}^{\mathrm{T}} = \{\epsilon_{11}, \epsilon_{22}, \epsilon_{12}\},$$
$$\{\epsilon^{\mathrm{n}}\}^{\mathrm{T}} = \{\epsilon_{13}, \epsilon_{23}\},$$

$$[B_{\mathrm{l}}^{\mathrm{p}}] = \begin{bmatrix} \partial_x & 0 & 0 \\ 0 & \partial_y & 0 \\ \partial_y & \partial_x & 0 \end{bmatrix}; \quad [B^{\mathrm{n}}] = \begin{bmatrix} \partial_z & 0 & \partial_x \\ 0 & \partial_z & \partial_y \end{bmatrix};$$

$$[B_{\mathrm{nl}}^{\mathrm{p}}] = \begin{bmatrix} 0 & 0 & \frac{u_{3,x}}{2}\partial_x \\ 0 & 0 & \frac{u_{3,y}}{2}\partial_y \\ 0 & 0 & \partial_y u_{3,x} + \partial_x u_{3,y} \end{bmatrix}.$$

A.1.2. Hooke's law

$$\{\sigma^{\mathrm{p}}\}_k^{\mathrm{T}} = \{\sigma_{11}^k, \sigma_{22}^k, \sigma_{12}^k\}, \quad \{\sigma^{\mathrm{n}}\}_k^{\mathrm{T}} = \{\sigma_{13}^k, \sigma_{23}^k\},$$

$$[C_{\mathrm{pp}}]_k = \begin{bmatrix} \bar{C}_{11} & \bar{C}_{12} & \bar{C}_{16} \\ \bar{C}_{12} & \bar{C}_{22} & \bar{C}_{26} \\ \bar{C}_{16} & \bar{C}_{26} & \bar{C}_{66} \end{bmatrix}_k; \quad [S_{\mathrm{nn}}]_k = \begin{bmatrix} S_{44} & S_{45} \\ S_{45} & S_{55} \end{bmatrix}_k,$$

where

$$\bar{C}_{ij} = C_{ij} - \frac{C_{i3}C_{3j}}{C_{33}} i, j = 1, 2, 6;$$
$$S_{44} = \frac{C_{55}}{\Delta}; \quad S_{55} = \frac{C_{44}}{\Delta};$$
$$S_{45} = \frac{C_{45}}{\Delta}; \quad \Delta = C_{44}C_{55} - C_{45}^2.$$

The relation between the stiffness coefficients C_{ij} (i, j = 1, 2, 6, 4, 5) and mechanical characteristic of the lamina (Young and shear moduli as well as Poisson coefficients) can be found in Ref. [40]. Naturally, these formula must be related to the θ_k orientation of the fibres in respect to the x-axis.

A.1.3. Displacement and stress models

$$\{X_{\mathrm{u}}\} = \{U_1^0, U_2^0, U_3^0, U_1^1, U_2^{1<}, D_1, D_2\},$$
$$\{X_\sigma\} = \{R_{1k}, R_{2k}, \sigma_{13}^{tk}, \sigma_{23}^{tk}, \sigma_{13}^{bk}, \sigma_{23}^{bk}\}.$$

The elements of the matrices $[E_{\mathrm{u}}]_k$ and $[E_\sigma]_k$ different by zero are:

$$E_{\mathrm{u}}^{11} = E_{\mathrm{u}}^{22} = E_{\mathrm{u}}^{33} = 1, \quad E_{\mathrm{u}}^{14} = E_{\mathrm{u}}^{25} = \frac{h}{2}\zeta,$$
$$E_{\mathrm{u}}^{16} = E_{\mathrm{u}}^{27} = (-1)^k\zeta_k \quad E_\sigma^{11} = E_\sigma^{22} = F_1,$$
$$E_\sigma^{13} = E_\sigma^{24} = F_0, \quad E_\sigma^{15} = E_\sigma^{26} = F_2.$$

The superscripts denote rows and columns of the considered matrices.

References

[1] Pagano JN. Exact solutions for composite laminates in cylindrical bending. J Composite Mat 1969;5:20–34.
[2] Carrera E. A class of two dimensional theories for anisotropic multilayered plates analysis. Accademia delle Scienze di torino. Mem. Sci. Fisiche 1995–96;19–20:49–89.
[3] Noor AK, Burton WS. Assessment of shear deformation theories for multilayered composite plates. Appl Mech Rev 1989;41:1–12.
[4] Kapania RK, Racita S. Recent advances in analysis of laminated beams and plates, part I: shear effects and buckling. Am Inst Aeronaut Astronaut 1989;27:923–34.
[5] Gaudenzi P, Barboni R, Mannini A. A finite element evaluation of single-layer and multi-layer theories for the analysis of laminated plates. Composite Struct 1995;30:427–40.
[6] Chia CY. Nonlinear analysis of anisotropic plates. New York: McGraw Hill, 1980.

[7] Chia CY. Geometrically nonlinear behaviour of composite plates: a review. Appl Mech Rev 1988;41:439–50.
[8] Kapania RK, Yang TY. Buckling, postbuckling, and nonlinear vibrations of imperfect plates. Am Inst Aeronaut Astronaut 1987;25:1338–46.
[9] Lay Z, Zhou RC, Xue DY, Huang JK, Mei C. Suppression of nonlinear panel flutter at elevate temperature with piezoelectric actuator. In: In: Proceedings of the AIAA/ASME/ASCE/AHS 34rd Structures, Structural Dynamics and Material Conference. La Jolla, CA, 1993:3466–74.
[10] Librescu L, Wang MY. Effects of geometric imperfections on vibrations of compressed shear deformable composite curved panels. Acta Mech 1993;97:203–24.
[11] Chandiramani NK, Plaut RH, Librescu LI. Non-linear flutter of buckled shear deformable-composite panels in a high-supersonic flow. Int J Non-linear Mech 1995;30:149–67.
[12] Nayfeh AH, Blanchandran B. 1995. Applied non linear dynamics. Series in Nonlinear Sciences. New York: Wiley.
[13] Ambartsumyan SA. Theory of anisotropic plates. Stanford, CT: Technomic, 1970.
[14] Hassert JE, Nowinski JL. Non-Linear transverse vibration of flat rectangular orthotropic plate supported by stiff ribs. In: Proceedings of the Fifth International Symposium on Space Technology and Science. Tokyo, 1962:561–70.
[15] Wu CI, Vinson JR. On non-linear oscillations of plates composed of composite materials. J Composite Mater 1969;3:548–61.
[16] Whitney JM, Leissa AW. Analysis of heterogeneous anisotropic plates. ASME, J Appl Mech 1969;36:261–66.
[17] Bert CW. Nonlinear vibration of rectangular plates arbitrarily laminated of anisotropic material. J Appl Mech 1973;40:452–58.
[18] Sathyamoorthy M. Nonlinear vibrations of plates: a review. Shock Vibrations Digest 1983;25:3–16.
[19] Sun CT, Chin H. On large defection effects in unsymmetric cross-ply composites laminates. J Composite Mater 1988;22:1045–59.
[20] Chandra R, Raju BB. Large amplitude flexural vibrations of crossply laminated composites plates. Fiber Sci Technol 1975;8:243–64.
[21] Singh G, Rao GV, Iyengar NGR. Large amplitude free vibration of simply-supported antisymmetric cross-ply plates. Am Inst Aeronaut Astronaut J 1991;29:784–90.
[22] Ganapathi M, Varadan TK, Sarma BS. Non-linear flexural vibration of laminated orthotropic plates. Comput Struct 1991;39:685–88.
[23] Di S, Ramm E. Hybrid stress formulation for higher order theory of laminated shell analysis. Comput Meth Appl Mech Engng 1993;109:359–76.
[24] Di S, Ramm E. Coupling of 2D- and 3D-composite shell elements in linear and nonlinear applications. Comput Meth Appl Mech Engng 1996;129:271–387.
[25] Reddy J, Chao WC. Non-linear oscillations of laminated anisotropic rectangular plates. J Appl Mech 1982;49:396–402.
[26] Kant T, Kommineni JR. Large amplitude free vibration analysis of cross-ply composite and sandwich laminates with a refined theory and C^0 finite elements. Comput Struct 1994;50:123–34.
[27] Zienkiewicz O. Finite element method. New York: McGraw-Hill, 1990.
[28] Hughes TJR. The finite element method. Englewood Cliffs, NJ: Prentice-Hall, 1987.
[29] Bathe KJ. Finite element—procedures in engineering analysis. Englewood Cliffs, NJ: Prentice-Hall, 1982.
[30] Palazotto AN, Dennis ST. Nonlinear analysis of shell structures. AIAA Series, 1992.
[31] Kröplin B, Dinkler D. Stabilitätstheorie. In: Mehlhorn G, editor. Handbuch für Bauingenieure. Berlin: Ernst & Sohn, 1994.
[32] Carrera E. C^0 Reissner–Mindlin multilayered plate elements including zig-zag and interlaminar stresses continuity. Presented at the Second EUROMECH Colloquium, Genova, 1994. Int J Numer Meth Engng 1996;39:1797–820.
[33] Murakami H. Laminated composite plate theory with improved in-plane response. J Appl Mech 1986;53:661–66.
[34] Carrera E, Kröplin B. Zig-zag and interlaminar equilibria effects in large deflection and postbuckling analysis of multilayered plates. Mech Composite Mater Struct 1997;4:69–94.
[35] Carrera E. An improved Reissner–Mindlin for the electromechanical analysis of multilayered structures including piezo-layers. J Intelligent Mater Systems Struct 1997;8:232–48.
[36] Reissner E. Note on the effect of the transverse shear deformation in laminated plates. Comput Meth Appl Mech Engng 1979;20:203–9.
[37] Carrera E. Large deflection behavior and incremental strategies in the FEM analysis of composite structures. ISD Bericht, University of Stuttgart, 1992.
[38] Carrera E. A study on arc-length-type methods and their operation failures illustrated by a simple model. Comput Struct 1994;50:217–29.
[39] Newmark NM. A method of computation for structural dynamics. J Engng Mech Div 1959;85:67–94.
[40] Jones RM. Mechanics of composite materials. New York: McGraw-Hill, 1975.
[41] Noor AK, Burton WS. Stress and free vibration analysis of multilayered composites plates. Composite Struct 1989;11:183–204.
[42] Chai CB, Banks WM, Rhodes J. An experimental study on laminated panels in compression. Composite Struct 1991;19:67–87.
[43] Carrera E. On the linear response of assymetrically laminated plates in cylindrical bending. Am Inst Aeronaut Astronaut J 1993;31(7):1353–57.
[44] Carrera E, Villonzo M. Large deflections and stability FEM analysis of shear deformable compressed anisotropic flat panels. Composite Struct 1994;29:433–44.
[45] Carrera E. Non Linear analysis of shear deformable plates. Int Council Aeronaut Sci 1994;3 (ICAS-94-9-8-2):2964–74.
[46] Carrera E, Villonzo M. On the effects of boundary conditions on postbuckling of compressed, symmetrically laminated, thick plates. Am Inst Aeronaut Astronaut J 1995;33:1543–46.